

PAPER • OPEN ACCESS

## Ultrafast photocarrier dynamics in InAs/GaAs self-assembled quantum dots investigated via optical pump-terahertz probe spectroscopy

To cite this article: Vince Paul Juguilon *et al* 2024 *J. Phys. D: Appl. Phys.* **57** 145107

View the [article online](#) for updates and enhancements.

You may also like

- [Charge carrier dynamics of GaAs/AlGaAs asymmetric double quantum wells at room temperature studied by optical pump terahertz probe spectroscopy](#)  
Jessica Afalla, Kaoru Ohta, Shunrou Tokonami *et al.*
- [Revealing charge carrier dynamics and transport in Te-doped GaAsSb and GaAsSbN nanowires by correlating ultrafast terahertz spectroscopy and optoelectronic characterization](#)  
Long Yuan, Rabin Pokharel, Shisir Devkota *et al.*
- [Intense terahertz radiation and their applications](#)  
H A Hafez, X Chai, A Ibrahim *et al.*

**PRIME**  
PACIFIC RIM MEETING  
ON ELECTROCHEMICAL  
AND SOLID STATE SCIENCE

HONOLULU, HI  
Oct 6-11, 2024

Abstract submission deadline:  
**April 12, 2024**

Learn more and submit!

**Joint Meeting of**  
The Electrochemical Society  
•  
The Electrochemical Society of Japan  
•  
Korea Electrochemical Society

# Ultrafast photocarrier dynamics in InAs/GaAs self-assembled quantum dots investigated via optical pump-terahertz probe spectroscopy

Vince Paul Juguilon<sup>1,\*</sup> , Deborah Anne Lumantas-Colades<sup>1</sup>, Karim Omambac<sup>2</sup> , Neil Irvin Cabello<sup>1</sup> , Inhee Maeng<sup>3</sup>, Chul Kang<sup>4</sup>, Armando Somintac<sup>1</sup> , Arnel Salvador<sup>1</sup>, Alexander De Los Reyes<sup>1</sup> , Chul-Sik Kee<sup>4</sup>  and Elmer Estacio<sup>1</sup> 

<sup>1</sup> National Institute of Physics, University of the Philippines Diliman, Quezon City, The Philippines

<sup>2</sup> University of Duisburg-Essen, Duisburg, North Rhine-Westphalia, Germany

<sup>3</sup> YUHS-KRIBB Medical Convergence Institute, Yonsei University College of Medicine, Seoul, Republic of Korea

<sup>4</sup> Advanced Photonics Research Institute, Gwangju Institute of Science and Technology, Gwangju, Republic of Korea

E-mail: [vjuguilon@nip.upd.edu.ph](mailto:vjuguilon@nip.upd.edu.ph)

Received 12 September 2023, revised 30 November 2023

Accepted for publication 22 December 2023

Published 19 January 2024



## Abstract

Optical pump-terahertz probe (OPTP) spectroscopy was performed to measure the lifetime of photogenerated carriers in the barrier and the wetting layer (WL) regions of an indium arsenide on gallium arsenide (InAs/GaAs) single-layer self-assembled quantum dot (QD) sample. A modified rate equation model of carrier dynamics was proposed where possible state-filling in both QD and WL is considered. Drude model fitting was also performed to extract the time-dependent plasma frequency and phenomenological scattering time from the terahertz transmission spectra. The results of the OPTP experiment show two prominent recombination processes that occur at different timescales after photoexcitation. These two processes were attributed to carrier recombination in the GaAs barrier and the quantum well-like states of the WL based on the fitted lifetimes. Calculations using the coupled differential rate equations were also able to replicate the experimental trend at low fluence. The lack of agreement between experimental data and numerical calculations at high optical fluence was mainly attributed to the possible saturation of the GaAs density of states. Lastly, the results of the parameter fitting for the plasma frequency and scattering time indicate a transition from the barrier to the WL recombination as the dominant carrier recombination mechanism within the time scale of the OPTP scan. This further lends credence to the proposed model for carrier dynamics in SAQD systems under state-filling conditions.

Keywords: quantum dots, carrier dynamics, rate equations, terahertz spectroscopy

\* Author to whom any correspondence should be addressed.



Original content from this work may be used under the terms of the [Creative Commons Attribution 4.0 licence](https://creativecommons.org/licenses/by/4.0/). Any further distribution of this work must maintain attribution to the author(s) and the title of the work, journal citation and DOI.

## 1. Introduction

Quantum dots (QDs) are nanoscale structures that exhibit three-dimensional quantum confinement of charge carriers [1]. This leads to the formation of discrete energy states, which give unique electronic and optical properties. Research has been conducted on these materials due to novel applications, which include solar cells, light-emitting diodes (LEDs), semiconductor lasers, and transistors [2–4].

Recent studies have demonstrated the use of optically-pumped III–V QD photonic crystal (PC) laser as a promising compact and low-energy consumption monolithic light sources for optical interconnects in silicon electronics and photonic integrated circuits [5, 6]. It has also been shown that QDs embedded in a semiconducting substrate can act as a viable emitter of terahertz (THz) radiation [7–10]. Terahertz emitters require materials with ultrafast carrier lifetime to improve the amplitude and bandwidth of the emitted THz radiation. Semiconductors such as low-temperature grown gallium arsenide (LT-GaAs) are often used due to the presence of midgap defects, which lower the lifetime of carriers [11]. However, these defect states decrease carrier mobility. Similarly, QDs grown on a semiconducting substrate known as self-assembled QDs (SAQD) can also act as ultrafast traps while maintaining relatively high carrier mobility [7, 8]. Thus, a fundamental understanding of carrier dynamics in QDs is necessary to optimize these potentials.

SAQDs are commonly grown through the Stranski-Krastanow (SK) method [12]. For indium arsenide on gallium arsenide (InAs/GaAs) QDs, the GaAs substrate is epitaxially grown, followed by one or two monolayers of the InAs material known as the wetting layer (WL). Upon reaching a critical thickness, it becomes more favorable for InAs to transition from layer-by-layer to island growth due to the lattice mismatch with the substrate. Three-dimensional confinement is then achieved by capping the structures with GaAs.

The ultrafast carrier dynamics in semiconductors may be investigated using an optical pump-terahertz probe (OPTP) spectroscopy setup. This technique allows for the nondestructive optical characterization and measurement of mobility and recombination lifetime of carriers in the picosecond to nanosecond timescale. In this experiment, an optical pump is used to generate photocarriers in the sample, which is then probed with a THz pulse after a short time delay. Since THz waves are sensitive to free carriers, information about carrier dynamics, such as carrier lifetime and photoconductivity, may be obtained by analyzing the THz transmittance over varying time delays between the optical pump and the THz probe [13, 14].

In this work, an InAs/GaAs SAQD sample was subjected to OPTP spectroscopy in an attempt to investigate the photo-generated carrier dynamics in the GaAs barrier and InAs WL region. A set of coupled differential rate equations was proposed based on published values for carrier relaxation, trapping, and recombination lifetimes in the GaAs barrier, InAs WL, and InAs QD regions. The numerical solutions for the

carrier densities obtained from the rate equations were compared with the measured decay characteristics from the OPTP experiment. Lastly, Drude model fitting was employed to verify possible changes in the recombination dynamics within the time scale of the OPTP scan.

## 2. Methodology

The sample was grown through the SK method using a RIBER-32P molecular beam epitaxy facility. An aluminum arsenide layer was grown in the thick GaAs buffer layer as a sacrificial layer for the epitaxial lift-off (ELO) process. The InAs dots have a growth rate of 0.136 monolayers/second at 540°C with an In:As<sub>4</sub> flux ratio of 1:261. The layer was capped with a Silicon-doped GaAs layer to achieve three-dimensional confinement of the carriers and as a protective layer. An uncapped sample variant with the same growth parameters was also prepared for atomic force microscopy (AFM) measurements. The grown QD epilayer was then transferred via ELO onto a magnesium oxide host layer, which is transparent in the THz frequencies. The cross-sectional schematic diagram of the sample is presented in figure 1.

Time-resolved THz spectroscopy was then conducted using an OPTP technique to observe the decay of photoexcited carriers. The diagram of the experimental setup is presented in figure 2. A Ti:sapphire laser with Spitfire® Ace™ regenerative amplifier was used as the excitation source, which emits ultrashort optical pulses at 800 nm wavelength with a pulse width of 35 fs and a repetition rate of 1 kHz. The laser beam was split into the optical pump and the THz probe lines using a beam splitter. The optical pump beam was focused onto the sample with a spot diameter of 3 mm. Terahertz radiation was emitted from a <110> zinc telluride (ZnTe) crystal via nonlinear optical rectification. Meanwhile, detection was achieved through the electro-optic (EO) sampling scheme. Both optical pump and THz probe beams were directed normal to the surface of the sample to measure the in-plane conductivity. The THz probe spot size was smaller than the optical beam to ensure homogenous sampling of the photoexcited surface. The setup was maintained in an airtight box to reduce THz wave absorption due to water vapor in free space.

The differential transmittance of the THz probe beam was measured by scanning the optical pump delay line while keeping the THz pump-probe delay centered at the peak of the time-domain THz waveform. The optical pump power was varied by adjusting a neutral density (ND) filter positioned along the beam path. The average optical power and the corresponding fluence are shown in table 1.

Terahertz transmission spectroscopy was also conducted while the sample was optically pumped using the highest and the lowest fluence to obtain the Drude complex conductivities. Global fitting was implemented by simultaneously fitting the real and imaginary parts of the complex conductivities to extract the plasma frequency and scattering time as fitting parameters.

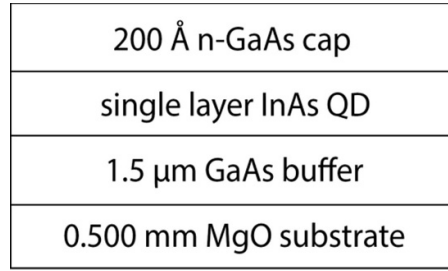


Figure 1. Schematic cross-section of the InAs/GaAs SAQD.

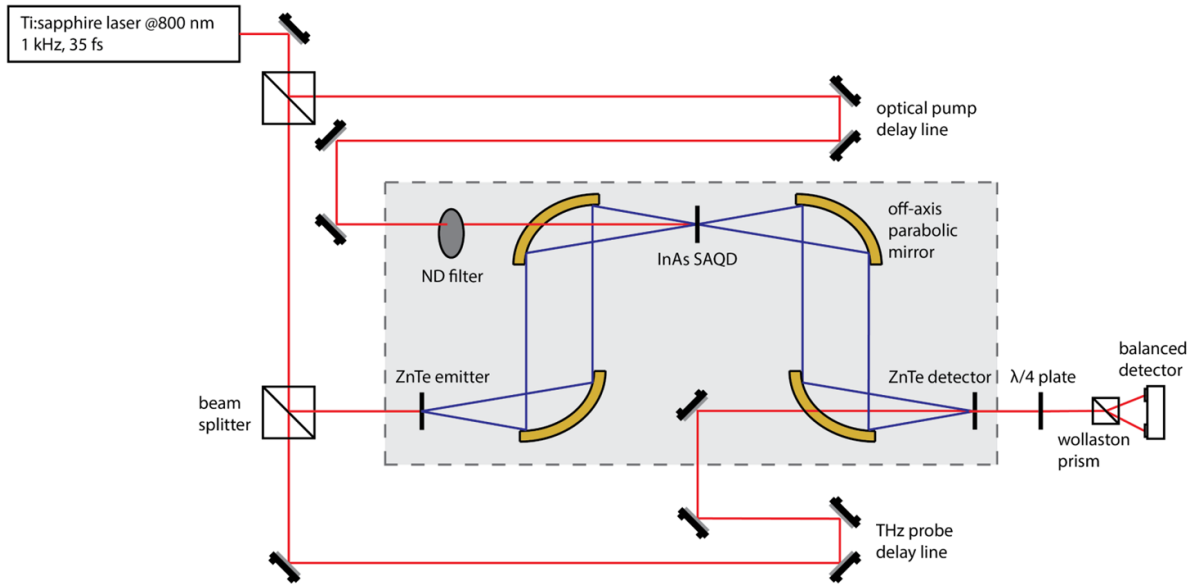


Figure 2. Experimental setup for the optical pump-terahertz probe spectroscopic analysis of the InAs/GaAs SAQD. Ultrashort optical pulses were generated by a Ti:sapphire laser with 35 fs pulse width and 1 kHz repetition rate.

Table 1. Average optical power used to photoexcite the sample, and the corresponding fluence calculated at 3 mm beam diameter, 800 nm wavelength, and 1 kHz repetition rate.

Average power (mW)	Fluence ( $\mu\text{J cm}^{-2}$ )
0.4	5.66
0.8	11.32
1.2	16.98
2.1	29.71
7.0	99.03

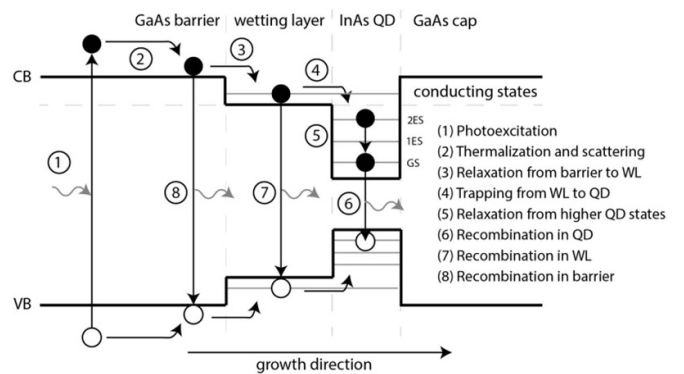


Figure 3. Photoexcited carrier dynamics in an InAs/GaAs SAQD system. Carriers are generated in the GaAs barrier and undergo subsequent relaxation and recombination.

### 3. Results and discussion

#### 3.1. Carrier dynamics in InAs/GaAs SAQD

Figure 3 illustrates the dynamical processes undergone by photocarriers in an InAs/GaAs SAQD system. The notation for lifetimes  $\tau_n$  used to describe these processes are indexed according to the process number shown in the diagram.

Photoexcitation occurs when the optical pump beam is incident on the sample, generating electron-hole pairs. Hot electrons (holes) may thermalize to the conduction band minimum (valence band maximum) and diffuse across the barrier region. The thermalization and scattering processes  $\tau_2$

occur within the order of hundreds of femtoseconds to several picoseconds [15]. Carriers may relax from the barrier region to the quantum well-like states of the WL with a lifetime of about  $\tau_3 = 2$  ps [16]. Carriers that are in the WL could also be trapped into the QD states with  $\tau_4 = 2$  ps [16]. State-filling of the WL and QD states is considered in this model, wherein the relaxation and trapping processes could only occur if there are free states in the WL and QD, respectively.

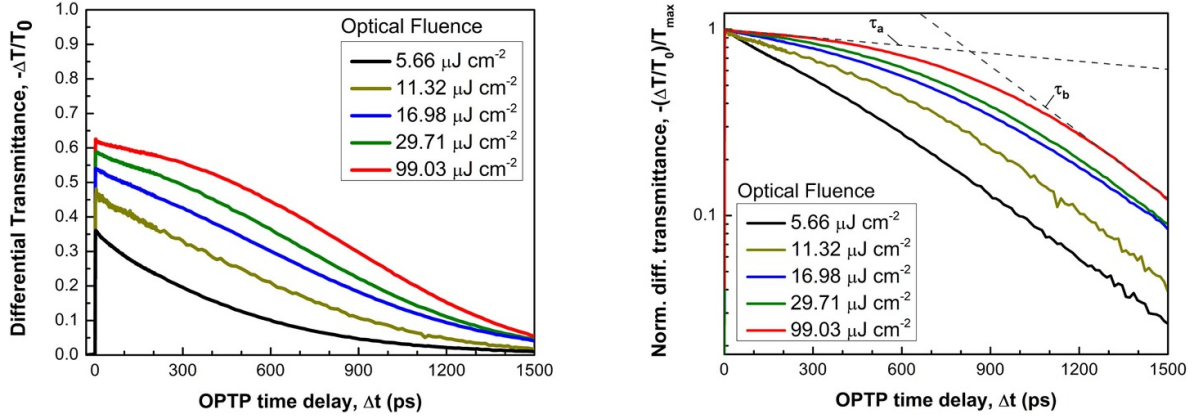


**Figure 4.** (a) Differential transmittance  $-\Delta T/T_0$  of the THz pulse through the InAs/GaAs SAQD as a function of the OPTP time delay  $\Delta t$  (b) The differential transmittance  $-\Delta T/T_0$  were normalized with respect to the maximum transmittance per curve  $T_{\text{max}}$  and expressed in a semi-log plot. Two distinct recombination processes with lifetimes  $\tau_a = 1900$  ps and  $\tau_b = 420$  ps were identified from the slope of the curves and were attributed to the barrier and WL recombination, respectively.

Subsequent carrier relaxation could occur from higher energy states in the QD through carrier–carrier or carrier-phonon interactions. Eventually, electron-hole pairs can recombine in the QD with a lifetime of  $\tau_6 = 2000$  ps [17]. Recombination is also possible in the WL and barrier regions with corresponding lifetimes of  $\tau_7 = 300$  ps and  $\tau_8$  within the range of 1000–2000 ps as measured from time-resolved photoluminescence spectroscopy experiments [18–21].

The possible thermal escape of electrons from the dots could also be considered with a low probability of occurrence due to the low energy associated with room temperature [22]. Several papers have also reported on a direct capture mechanism of carriers from barrier to QD [8, 23].

### 3.2. OPTP spectroscopy

Since THz waves are sensitive to free carriers, the THz transmitted intensity will decrease in proportion to the free carrier concentration. These include carriers that occupy the GaAs barrier ( $n_B$ ) and the InAs WL ( $n_W$ ) regions [24, 25]. Carriers trapped in the dots ( $n_D$ ) are relatively immobile due to three-dimensional confinement [9, 25]. Thus, free carrier decay may be investigated by measuring the THz transmittance as a function of time delay  $\Delta t$  between the optical pump and THz probe.

Figure 4(a) shows the differential transmittance  $\Delta T/T_0$  for the different optical pump fluence. Here,  $\Delta T$  is defined as  $T(\Delta t) - T_0$  where  $T(\Delta t)$  is the amplitude of the TDS waveform as function of the OPTP time delay  $\Delta t$ . This is then normalized with respect to the peak amplitude  $T_0$  of the TDS waveform for the case of no optical pump. At low differential transmittance,  $\Delta T/T_0$  may be related to the photoinduced conductivity according to equation (1) [26–28].

$$\sigma = \frac{N+1}{Z_0 d} \left| \frac{\Delta T}{T_0} \right| \quad (1)$$

where  $N$  is the refractive index of the sample,  $Z_0$  the impedance of free space, and  $d$  the penetration depth of the optical pulse. Due to the higher mobility of electrons compared to holes, the

contribution of electrons will be more significant in increasing the conductivity, as seen in equation (2). Hence, the differential transmittance may be related to the electron density

$$\sigma = e\mu_e n_e. \quad (2)$$

The differential transmittance was then normalized with respect to the maximum transmittance value per fluence  $T_{\text{max}}$ . These were expressed as semi-log plots in figure 4(b) to identify the possible dynamical processes that occur during the time scale of the OPTP scan. In this plot, the slope of the curve is inversely proportional to the effective carrier lifetime. The linearized plots presented in figure 4(b) indicate two prominent carrier dynamics that occur during the measurement timescale: a recombination process with a lifetime of about  $\tau_a = 1900$  ps, and relatively faster carrier recombination with a lifetime of around  $\tau_b = 420$  ps. These dynamical processes were attributed to the GaAs barrier and InAs WL recombination, respectively, based on the range of literature values. Moreover, the faster WL recombination process appeared to be the sole carrier decay mechanism at 5.66  $\mu\text{J cm}^{-2}$  optical fluence as denoted by the single slope observed from the linearized curve. A fluence-dependent dynamical process may be observed within the first several hundred picoseconds, where a higher fluence corresponds to a decrease in the slope, which further implies a slower effective carrier recombination lifetime. Eventually, the slopes of the curves increase and start to approach that of the lowest fluence. This transition in the recombination dynamics occurs at about  $\Delta t = 800$  ps for the highest optical fluence used in the experiment.

### 3.3. Numerical simulation using rate equation model

A rate equation model was proposed based on coupled-differential equations of the carrier dynamics described in figure 3. Possible state-filling of both QD and WL states was considered in this numerical model [23, 29].

**Table 2.** Numerical values of the parameters used in the modified rate equation model.

Parameter	Significance	Value
$\tau_3$	barrier-WL relaxation time	2 ps
$\tau_4$	WL-QD trapping time	2 ps
$\tau_6$	QD recombination time	2000 ps
$\tau_7$	WL recombination time	420 ps
$\tau_8$	barrier recombination time	1900 ps
$n_W^{\text{sat}}$	WL carrier saturation	$1.40 \times 10^{13} \text{ cm}^{-2}$
$n_D^{\text{sat}}$	QD carrier saturation	$1.56 \times 10^{11} \text{ cm}^{-2}$

The differential equations for the barrier ( $n_B$ ), WL ( $n_W$ ), and QD ( $n_D$ ) regions are presented in equations (3)–(5).

$$\frac{dn_B}{dt} = -\frac{n_B}{\tau_8} - \frac{n_B}{\tau_3} \left(1 - \frac{n_W}{n_W^{\text{sat}}}\right) \quad (3)$$

$$\frac{dn_W}{dt} = -\frac{n_W}{\tau_7} - \frac{n_W}{\tau_4} \left(1 - \frac{n_D}{n_D^{\text{sat}}}\right) + \frac{n_B}{\tau_3} \left(1 - \frac{n_W}{n_W^{\text{sat}}}\right) \quad (4)$$

$$\frac{dn_D}{dt} = -\frac{n_D}{\tau_6} + \frac{n_W}{\tau_4} \left(1 - \frac{n_D}{n_D^{\text{sat}}}\right). \quad (5)$$

The parameters used in the rate equation model and their corresponding numerical values are summarized in table 2.

Equation (3) represents the carrier dynamics in the barrier region. The first term indicates a radiative recombination with a lifetime of  $\tau_8 = 1900$  ps [18]. The second term is the relaxation into the WL with  $\tau_3 = 2$  ps [16]. Possible state filling is considered in the WL region with a saturation value of  $n_W^{\text{sat}}$ .

Equation (4) shows carrier trapping and recombination in the WL. The first term is a radiative recombination process with a corresponding lifetime of  $\tau_7 = 420$  ps [18, 19]. The second term represents carrier trapping into the QDs, where possible state-filling of QD energy states is also considered. Photoluminescence spectroscopy conducted by Omambac *et al* shows three distinct peaks corresponding to the recombination in the ground state and the first- and second-excited states [30]. The QD carrier density saturation value  $n_D^{\text{sat}}$  is then given by

$$n_D^{\text{sat}} = 6n_D^{\text{AFM}} \quad (6)$$

where  $n_D^{\text{AFM}} = 2.60 \times 10^{10} \text{ cm}^{-2}$  is the dot density measured using AFM, with an additional prefactor of 2 to denote that each energy state in the dot can accommodate two electrons with opposite spins [23].

Lastly, equation (5) represents dynamics for carriers trapped in the dots. The effective recombination rate for the three energy states is characterized by a single carrier decay process with a lifetime  $\tau_6 = 2000$  ps [17].

Equations (3)–(5) were numerically solved using the ODEINT function of the SciPy package to obtain the time-dependent carrier density for the barrier, WL, and QD regions.

The WL saturation was set as a free fitting parameter. The decay of photoconducting carriers was also linearized and

superimposed with experimental data, as shown in figure 5. The proposed rate equation model shows good agreement with the observed experimental trend at low optical fluence. A WL saturation value of  $1.40 \times 10^{13} \text{ cm}^{-2}$  was obtained from fitting [31]. According to the proposed model, carriers generated in the barrier will occupy the lowest available energy state in the QD and WL through ultrafast processes. Results of the calculations, summarized in table 3, indicate that carriers generated from the  $5.66 \mu\text{J cm}^{-2}$  photon flux at 800 nm will lead to state-filling of the QD energy states. Hence, the majority of carriers will be occupied in the WL. At this fluence, WL recombination will be the dominant dynamical process signified by the single slope measured from the linearized differential transmittance.

As the optical fluence is increased beyond the WL saturation value, the ultrafast barrier-to-WL relaxation process will terminate due to state-filling in the WL region (described in equation (2)), and photogenerated carriers will occupy both the InAs WL and GaAs barrier regions. The slower carrier recombination in the GaAs barrier region will increase the effective recombination lifetime, which corresponds to a decreased slope in the linearized differential transmittance curves. Further increase of the optical fluence would also result in a higher carrier density in the barrier region, which will cause the barrier recombination to dominate over WL recombination and could lead to a higher effective lifetime. Eventually, the total photogenerated carrier density in the sample would decrease over time due to recombination until there are only enough carriers to fill the WL region. As this occurs, the underlying WL recombination will re-emerge as the dominant mechanism for carrier recombination. This transition from barrier- to WL-dominant recombination could be seen as the change in slope, which occurs at  $\Delta t = 800$  ps for the  $99.03 \mu\text{J cm}^{-2}$  differential transmittance curve.

Meanwhile, the rate equation model at high optical fluence led to an overestimation of the generated carrier density compared to experimental data, as observed from both the 29.71 and  $99.03 \mu\text{J cm}^{-2}$  transmittance curves. Table 3 suggests that the calculated photon flux at these fluence values will generate a carrier density that is significantly greater than the GaAs density of states (DOS) ( $4.7 \times 10^{17} \text{ cm}^{-3}$ ). Hence, the optical pump could no longer generate photoexcited carriers due to the limited number of states in the GaAs conduction band. This is supported by the extended plot of the rate equation model reported in figure 5(b), where the expected transition in the recombination dynamics at high excitation fluence is seen to occur at a later time. This could suggest a higher initial carrier density in the simulations, compared to the OPTP experiment where the photogenerated carrier density is limited by the GaAs DOS. Additionally, the thermal energy introduced by the optical pump beam would also cause sample heating. This could lead to the thermal escape of electrons from the dots, which would be significant at higher fluence. However, the good agreement of experimental data with the proposed rate equation model without the thermal contribution term may suggest that this process could be insignificant even at the high fluence values considered [22].

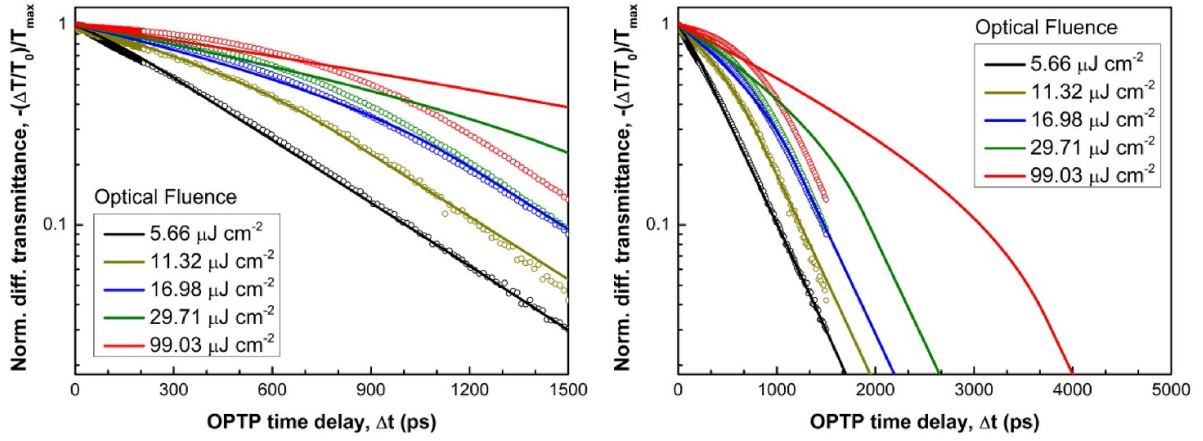


**Figure 5.** (a) Simulations of the proposed model (solid lines) show good agreement with the OPTP data (scatter) at low fluence. (b) An extended plot of the simulations indicates that changes in carrier dynamics for the 29.71 and 99.03  $\mu\text{J cm}^{-2}$  optical excitation fluence values occur at a later time compared to experimental data.

**Table 3.** Optical properties of the pump beam with 1 kHz repetition rate, 35 fs pulse width, 800 nm wavelength, 3 mm beam diameter, and 1  $\mu\text{m}$  penetration depth in GaAs.

Optical fluence ( $\mu\text{J cm}^{-2}$ )	Photon flux ( $\text{cm}^{-2}$ )	Generated carrier density ( $\text{cm}^{-3}$ )
5.66	$2.28 \times 10^{13}$	$2.28 \times 10^{17}$
11.32	$4.56 \times 10^{13}$	$4.56 \times 10^{17}$
16.98	$6.84 \times 10^{13}$	$6.84 \times 10^{17}$
29.71	$1.20 \times 10^{14}$	$1.20 \times 10^{18}$
99.03	$3.99 \times 10^{14}$	$3.99 \times 10^{18}$

### 3.4. Drude conductivity

The THz time-domain transmission spectra were obtained by scanning the THz pump-probe delay at a fixed delay time  $\Delta t$  between the arrival of the optical pump and the terahertz probe beams. Time-domain waveforms and the corresponding Fourier transforms are presented in figure 6 for optical excitation fluence values of 5.66 and 99.03  $\mu\text{J cm}^{-2}$ .

The decrease in the THz peak amplitude is due to free carrier absorption and the increased photoconductivity of the sample upon optical excitation. A longer delay between the arrival of the pump and probe beams would allow electron-hole pairs to recombine, which decreases carrier density and equates to a higher peak amplitude. Thus, minimum transmittance is expected at  $\Delta t = 0$  when both optical pump and THz probe are simultaneously incident on the sample. A reference TDS transmission spectra with no optical excitation is also presented in the plots.

The frequency-dependent transmittance  $\tilde{T}(\omega)$  may be related to the transmitted THz field  $\tilde{E}_p(\omega, \Delta t)$  at a given OPTP delay time and the reference scan  $\tilde{E}_{\text{ref}}(\omega)$  by [32]

$$\tilde{T}(\omega) = |T| e^{i\phi} = \frac{\tilde{E}_p(\omega, \Delta t)}{\tilde{E}_{\text{ref}}(\omega)}. \quad (7)$$

From the transmission amplitude  $|T|$  and phase  $\phi$ , both real  $\sigma'(\omega)$  and imaginary  $\sigma''(\omega)$  parts of the complex conductivity may be calculated according to equations (8) and (9) [33].

$$\sigma'(\omega, \Delta t) = \frac{N_{\text{GaAs}} + 1}{Z_0 d} \left( \frac{1}{|T|} \cos \phi - 1 \right) \quad (8)$$

$$\sigma''(\omega, \Delta t) = -\frac{N_{\text{GaAs}} + 1}{Z_0 d} \left( \frac{1}{|T|} \sin \phi \right) \quad (9)$$

where  $Z_0 = 377 \Omega$  is the impedance of free space,  $N_{\text{GaAs}} = 3.6$  is the refractive index of both GaAs and InAs in the THz region, and  $d = 1 \mu\text{m}$  is the penetration depth of the 800 nm optical pulse [34, 35].

Global fitting was performed for the real and imaginary parts of the complex conductivity as shown in figure 7. From the Drude model, the complex conductivity  $\tilde{\sigma}$  is given by

$$\tilde{\sigma}(\omega, \Delta t) = \frac{\varepsilon_0 \omega_p^2 \tau_s}{1 - i\omega \tau_s} \quad (10)$$

where  $\omega_p$  is the plasma frequency and  $\tau_s$  the phenomenological scattering time. Both plasma frequency  $\omega_p$  and scattering time  $\tau_s$  were obtained as fitting parameters. The plasma frequency is related to the total photocarrier density  $n_{\text{exc}}$  through the dielectric constant of free space  $\varepsilon_0$  and the electron effective mass in GaAs  $m_e^*$ .

$$\omega_p^2 = \frac{n_{\text{exc}} e^2}{\varepsilon_0 m_e^*}. \quad (11)$$

According to [36], using the GaAs effective mass for both GaAs and InAs regions leads to similar electron subbands in strained InAs/GaAs superlattice structures.

A carrier density of  $n_{\text{exc}} = 2.11 \times 10^{17} \text{ cm}^{-3}$  was obtained from the plasma frequency at 5.66  $\mu\text{J cm}^{-2}$  optical fluence and  $\Delta t = 0$  ps. This value was in close agreement with the calculated photogenerated carrier density shown in table 3. Meanwhile, a carrier density of  $7.97 \times 10^{17} \text{ cm}^{-3}$  was calculated for an excitation fluence of 99.03  $\mu\text{J cm}^{-2}$  at  $\Delta t = 0$  ps,

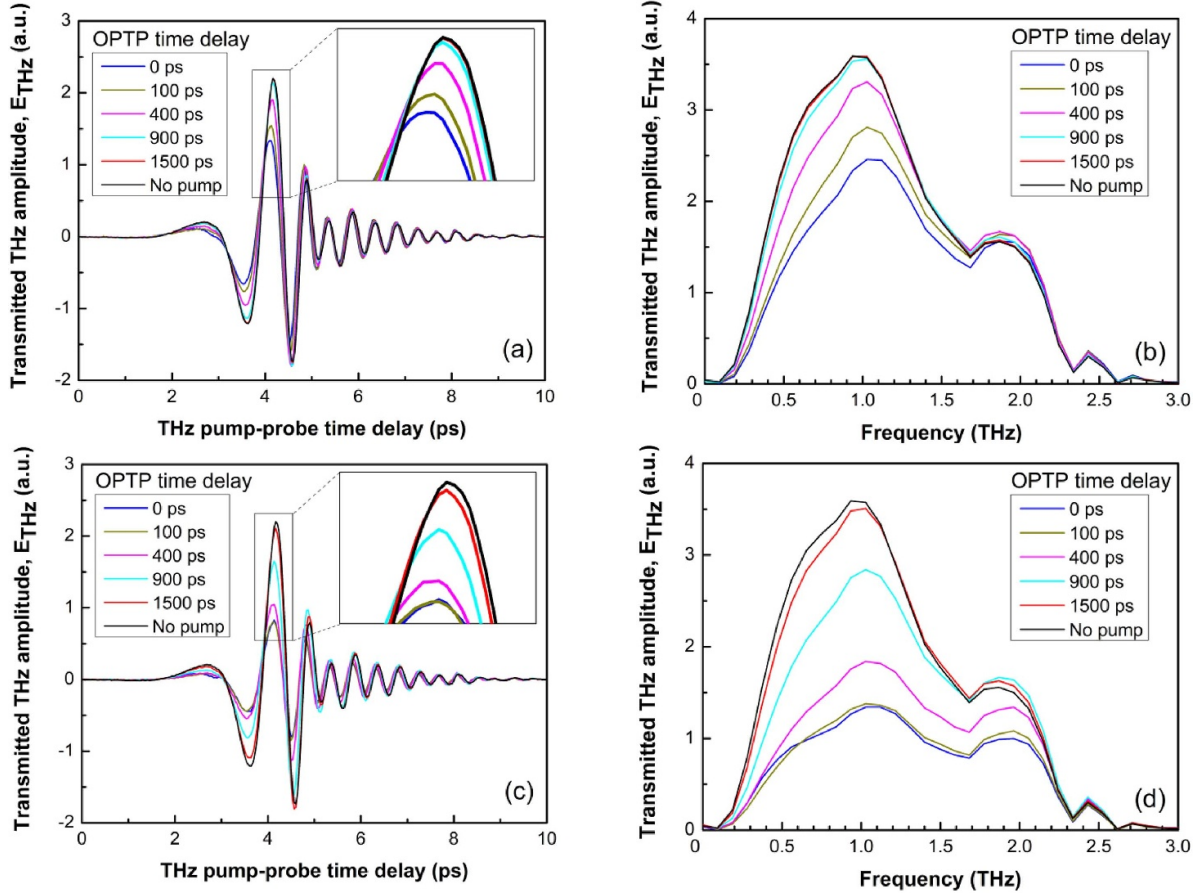


**Figure 6.** The THz time-domain transmission spectra and corresponding FFT spectra at  $5.66 \mu\text{J cm}^{-2}$  optical fluence are presented in (a) and (b). Similarly, (c) and (d) show both the time-domain and frequency-domain spectra at  $99.03 \mu\text{J cm}^{-2}$  optical excitation fluence for different optical pump-terahertz probe delay times.

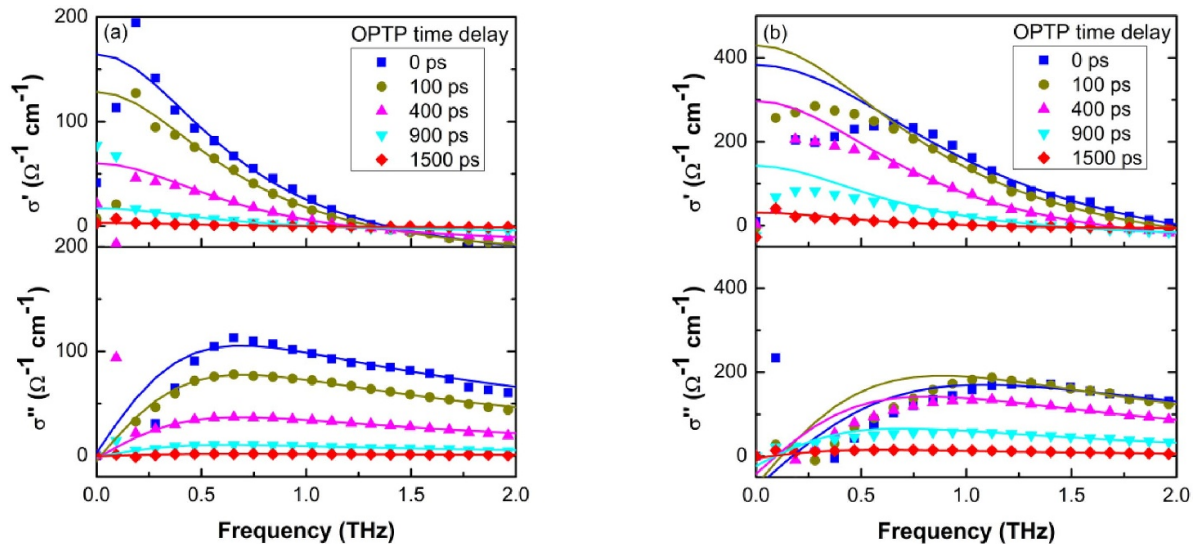


**Figure 7.** The real  $\sigma'$  and imaginary  $\sigma''$  parts of the complex conductivities (scatter) for the (a)  $5.66 \mu\text{J cm}^{-2}$  and the (b)  $99.03 \mu\text{J cm}^{-2}$  optical excitation fluence were globally-fitted (solid) to obtain the plasma frequency.

which is less than the density generated by the optical pump and could indicate the effective GaAs DOS of the particular sample.

The plasma frequency  $\omega_p(\Delta t = 0)$  immediately upon photoexcitation with the  $5.66 \mu\text{J cm}^{-2}$  fluence is highlighted in figure 8 to represent the WL carrier saturation level.

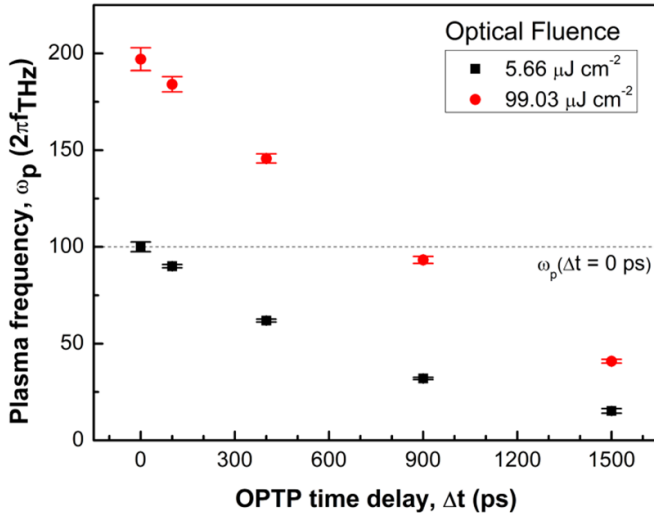


**Figure 8.** The time-dependent plasma frequency is related to the photocarrier density. The plasma frequency for  $5.66 \mu\text{J cm}^{-2}$  fluence at  $\Delta t = 0$  ps represents WL saturation value.

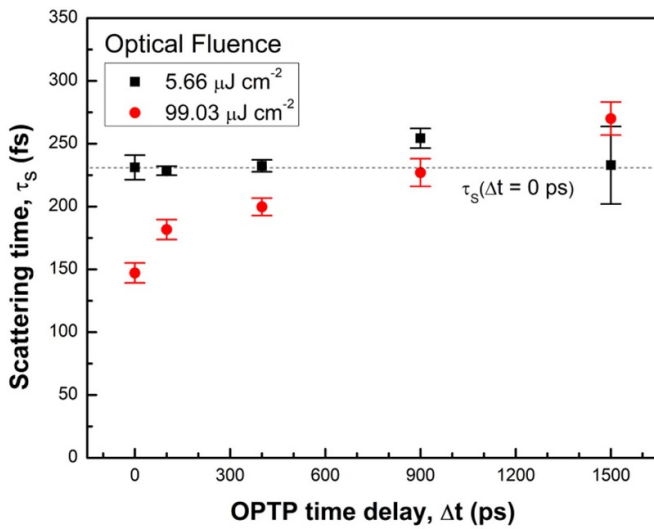


**Figure 9.** Scattering time of the photogenerated carriers in the SAQD sample obtained from Drude global fitting.

Photogenerated carriers beyond this value will be occupied in the GaAs barrier as in the case of the  $99.03 \mu\text{J cm}^{-2}$  excitation fluence. Extrapolating between the data points of the high fluence case suggests that the total carrier density reached the highlighted level at about  $\Delta t = 800$  ps. As discussed previously, the total photocarrier density in the sample is only sufficient to occupy the WL states, and a WL-dominated recombination process occurs based on the slopes in figures 5(a) and (b) for the time frame  $\Delta t > 800$  ps.

This change in carrier dynamics was also seen in figure 9, where the scattering time of the sample optically-excited by the  $5.66 \mu\text{J cm}^{-2}$  pump remained relatively constant at around 230–250 fs, indicating relatively high carrier mobility in the WL region [37].

Meanwhile, the scattering time at  $99.03 \mu\text{J cm}^{-2}$  fluence was initially measured at 150 fs, which is within the reported value for  $\tau_s$  in bulk GaAs [32]. This could suggest that most carriers reside in the barrier region at high excitation fluence. The observed increase in scattering time would signify a transition from the barrier to the WL as the dominant carrier recombination site at about  $\Delta t = 800$  ps. At this point, most of the remaining photocarriers would now reside in the WL region.

#### 4. Conclusions

Ultrafast carrier dynamics in InAs/GaAs SAQDs were investigated using OPTP spectroscopy. Results of the experiment indicate that the photocarriers could recombine at the barrier and WL regions within the time scale of the OPTP scan. The dynamical processes were also modeled by modified differential rate equations, which consider possible state-filling in the QD and WL regions. Simulations show relatively good agreement with the observed trend at low optical fluence. In this model, carriers are generated in the barrier region and could occupy the lowest available energy state in the QD and WL through ultrafast relaxation and trapping. Calculations suggest that the majority of carriers generated at  $5.66 \mu\text{J cm}^{-2}$  optical fluence will occupy and could saturate the WL region states. Thus, a single carrier decay process can be measured at this fluence, which corresponds to WL recombination. As the excitation fluence increases, WL saturation will occur, and carriers could start to populate the GaAs barrier. This increases the carrier effective lifetime due to the relatively longer barrier recombination ( $\tau_8 = 1900$  ps) as compared to the WL ( $\tau_7 = 420$  ps). Over time, carrier recombination would decrease the total photocarrier concentration until there are only sufficient carriers to occupy the WL region. As this occurs, the WL recombination will be the dominant recombination process.

The numerical simulations at high excitation fluence did not agree with the OPTP experimental data. Calculations show that the photogenerated carrier density will be greater than the GaAs conduction band DOS for both  $29.71$  and  $99.03 \mu\text{J cm}^{-2}$  excitation fluence. This leads to the saturation of the GaAs conduction band states, which was not accounted for in the rate equations. Additionally, the sample heating due to the thermal energy introduced by the optical pump would be significant at these fluence values, which would cause the thermal escape of electrons from the QDs.

Both plasma frequency  $\omega_p$  and phenomenological scattering time  $\tau_s$  were obtained as fitting parameters from the Drude global fitting of the real and imaginary parts of the complex conductivity. The corresponding photogenerated carrier density obtained from the plasma frequency at  $99.03 \mu\text{J cm}^{-2}$  was lower than the calculated value using the photon flux. This supports the premise that GaAs barrier state-filling could have occurred at high optical fluence. Moreover, the transition from barrier to WL recombination as the carrier recombination mechanism was observed at  $\Delta t = 800$  ps using the data from both time delay-dependent plasma frequency and scattering

time. This change in dynamics is also reflected in the results for the differential transmittance from the OPTP experiment.

It was noted that the method used in this study was limited to probing the free carrier dynamics in the GaAs barrier and WL region since carriers in the QD are confined. Moreover, the ultrafast processes, such as relaxation and trapping, could not be identified in the OPTP data due to limitations in the resolution of the scan. These processes are expected to occur within the first several picoseconds upon photoexcitation. The rate equation models could also be further improved by considering additional processes and pathways for carriers, such as trapping into the defect or surface states, Auger recombinations, or thermal escape from QDs. This could provide additional insights into how each specific recombination process proceeds at the onset of saturation. The addition of a thermal excitation term in the rate equation would also give a more accurate numerical model of the charge carrier dynamics due to the sample heating that occurs as a result of the optical pump. Nonetheless, the good agreement between OPTP data compared with numerical results of the proposed rate equation model, even as the fluence is increased, suggests that the thermal contribution could be minimal.

The key similarities that had been observed between the OPTP experimental results, numerical calculations using the modified rate equations model, and Drude model global fitting, along with the close agreement with published values, lend proof to the feasibility of the proposed model in accurately describing the dynamical processes which occur in an InAs/GaAs SAQD system, particularly at the onset of optical saturation. This would have implications for several practical applications since the optical saturation threshold is vital in the design and evaluation of the overall efficiency of QD-based LEDs, photovoltaic cells, or semiconductor lasers.

### Data availability statement

All data that support the findings of this study are included within the article (and any supplementary files).

### Acknowledgments

This work was supported in part by the Department of Science and Technology—Philippine Council for Industry, Energy, and Emerging Technology Research and Development—Grants in Aid (DOST PCIEERD-GIA Project No. 11336).

### ORCID iDs

Vince Paul Juguilon  <https://orcid.org/0009-0005-6509-3257>

Karim Omambac  <https://orcid.org/0000-0002-5013-9567>

Neil Irvin Cabello  <https://orcid.org/0000-0002-0988-7184>

Armando Somintac  <https://orcid.org/0000-0002-5285-4505>

Alexander De Los Reyes  <https://orcid.org/0000-0003-2432-0669>

Chul-Sik Kee  <https://orcid.org/0000-0002-3219-5119>

Elmer Estacio  <https://orcid.org/0000-0002-4938-571X>

### References

- [1] Harrison P and Valavanis A 2016 *Quantum Wells Wires and Dots: Theoretical and Computational Physics of Semiconductor Nanostructures* (Wiley)
- [2] Nozik A J 2002 Quantum dot solar cells *Physica E* **14** 115–20
- [3] Shang C, Wan Y, Selvidge J, Hughes E, Herrick R, Mukherjee K, Duan J, Grillot F, Chow W W and Bowers J E 2021 Perspectives on advances in quantum dot lasers and integration with Si photonic integrated circuits *ACS Photonics* **8** 2555–66
- [4] Hetsch F, Zhao N, Kershaw S V and Rogach A L 2013 Quantum dot field effect transistors *Mater. Today* **16** 312–25
- [5] Zhou T *et al* 2020 Continuous-wave quantum dot photonic crystal lasers grown on on-axis Si (001) *Nat. Commun.* **11** 977
- [6] Kosciwa R, Wan Y, He W, Kennedy M J and Bowers J E 2023 Heterogeneous integration of a III–V quantum dot laser on high thermal conductivity silicon carbide *Opt. Lett.* **48** 2539–42
- [7] Turchinovich D, Pierz K and Uhd Jepsen P 2003 InAs/GaAs quantum dots as efficient free carrier deep traps *Phys. Status Solidi C* **15** 56–9
- [8] Gorodetsky A, Bazieva N and Rafailov E U 2019 Pump dependent carrier lifetimes in InAs/GaAs quantum dot photoconductive terahertz antenna structures *J. Appl. Phys.* **125** 151606
- [9] Presto J M M, Prieto E A P, Omambac K M, Afalla J P C, Lumantas D A O, Salvador A A, Somintac A S, Estacio E S, Yamamoto K and Tani M 2015 Confined photocarrier transport in InAs pyramidal quantum dots via terahertz time-domain spectroscopy *Opt. Express* **23** 14532–40
- [10] De Los Reyes A E, Vasquez J D, Bardolaza H R, Lopez L P, Chang C-Y, Somintac A S, Salvador A A, Jang D-J and Estacio E S 2020 Low-temperature carrier dynamics in MBE-grown InAs/GaAs single- and multi-layered quantum dots investigated via photoluminescence and terahertz time-domain spectroscopy *Opt. Mater. Express* **10** 178
- [11] Escaño M C *et al* 2020 True bulk As-antisite defect in GaAs(110) identified by DFT calculations and probed by STM/STS measurements *Appl. Surf. Sci.* **511** 145590
- [12] Baskaran A and Smereka P 2012 Mechanisms of Stranski-Krastanov growth *J. Appl. Phys.* **111** 044321
- [13] Kang C, Lee G, Lee W-J, Cho D-H, Maeng I, Chung Y-D and Kee C-S 2021 Terahertz emission and ultrafast carrier dynamics of Ar-ion implanted Cu(In, Ga)Se thin films *Crystals* **11** 411
- [14] Beard M C, Turner G M and Schmuttenmaer C A 2000 Transient photoconductivity in GaAs as measured by time-resolved terahertz spectroscopy *Phys. Rev. B* **62** 15764–77
- [15] Newmeyer E-R, North J D and Swearer D F 2022 Hot carrier photochemistry on metal nanoparticles *J. Appl. Phys.* **132** 230901
- [16] Li Q, Xu Z Y and Ge W K 2000 Carrier capture into InAs/GaAs quantum dots detected by a simple degenerate pump–probe technique *Solid State Commun.* **115** 105–8
- [17] Tang Y, Rich D H, Mukhametzhanov I, Chen P and Madhukar A 1998 Self-assembled InAs/GaAs quantum

- dots studied with excitation dependent cathodoluminescence *J. Appl. Phys.* **84** 3342–8
- [18] Yarotski D A, Averitt R D, Negre N, Crooker S A, Taylor A J, Donati G P, Stintz A, Lester L F and Malloy K J 2002 Ultrafast carrier-relaxation dynamics in self-assembled InAs/GaAs quantum dots *J. Opt. Soc. Am. B* **19** 1480
- [19] Herz L M, Phillips R T, Le Ru E C and Murray R 2002 Time-resolved photoluminescence cross-correlation measurements on InAs quantum dots *Phys. Status Solidi A* **190** 565–9
- [20] Wang H L, Yang F H, Feng S L, Zhu H J, Ning D, Wang H and Wang X D 2000 Experimental determination of local strain effect on InAs/GaAs self-organized quantum dots *Phys. Rev. B* **61** 5530–4
- [21] Marcinkevičius S and Leon R 2000 Photoexcited carrier transfer in InGaAs quantum dot structures: dependence on the dot density *Appl. Phys. Lett.* **76** 2406–8
- [22] Sanguinetti S, Henini M, Grassi Alessi M, Capizzi M and Franchi S 1999 Carrier thermal escape and retrapping in self-assembled quantum dots *Phys. Rev. B* **60** 8276–83
- [23] de Sales F V, Cruz J M R, da Silva S W, Soler M A G, Morais P C, da Silva M J, Quivy A A and Leite J R 2003 Coupled rate equation modeling of self-assembled quantum dot photoluminescence *Microelectron. J.* **34** 705–7
- [24] Porte H P, Uhd Jepsen P, Daghestani N, Rafailov E U and Turchinovich D 2009 Ultrafast release and capture of carriers in InGaAs/GaAs quantum dots observed by time-resolved terahertz spectroscopy *Appl. Phys. Lett.* **94** 262104
- [25] Oh S J, Kang C, Maeng I, Son J-H, Cho N K, Song J D, Choi W J, Cho W-J and Lee J I 2007 Measurement of carrier concentration captured by InAs/GaAs quantum dots using terahertz time-domain spectroscopy *Appl. Phys. Lett.* **90** 131906
- [26] Cooke D G, Hegmann F A, Mazur Y I, Ma W Q, Wang X, Wang Z M, Salamo G J, Xiao M, Mishima T D and Johnson M B 2004 Anisotropic photoconductivity of InGaAs quantum dot chains measured by terahertz pulse spectroscopy *Appl. Phys. Lett.* **85** 3839–41
- [27] Lui K P H and Hegmann F A 2001 Ultrafast carrier relaxation in radiation-damaged silicon on sapphire studied by optical-pump–terahertz-probe experiments *Appl. Phys. Lett.* **78** 3478–80
- [28] Hegmann F A, Tykwinski R R, Lui K P H, Bullock J E and Anthony J E 2002 Picosecond transient photoconductivity in functionalized pentacene molecular crystals probed by terahertz pulse spectroscopy *Phys. Rev. Lett.* **89** 227403
- [29] Shamirzaev T S, Abramkin D S, Nenashev A V, Zhuravlev K S, Trojáněk F, Dzurnák B and Malý P 2010 Carrier dynamics in InAs/AlAs quantum dots: lack in carrier transfer from wetting layer to quantum dots *Nanotechnology* **21** 155703
- [30] Omambac K M, Porquez J G, Afalla J, Vasquez D and Salvador A A 2013 Application of external tensile and compressive strain on a single layer InAs/GaAs quantum dot via epitaxial lift-off *Phys Status Solidi* **250** 1632–5
- [31] Cappelluti F, Gioannini M and Khalili A 2016 Impact of doping on InAs/GaAs quantum-dot solar cells: a numerical study on photovoltaic and photoluminescence behavior *Sol. Energy Mater. Sol. Cells* **157** 209–20
- [32] Afalla J et al 2017 Charge carrier dynamics of GaAs/AlGaAs asymmetric double quantum wells at room temperature studied by optical pump terahertz probe spectroscopy *Jpn. J. Appl. Phys.* **56** 111203
- [33] Cunningham P D 2013 Accessing terahertz complex conductivity dynamics in the time-domain *IEEE Trans. Terahertz Sci. Technol.* **3** 494–8
- [34] Mendis R, Smith M L, Bignell L J, Vickers R E M and Lewis R A 2005 Strong terahertz emission from (100) p-type InAs *J. Appl. Phys.* **98** 126104
- [35] Shi Y, Zhou Q-L, Zhang C and Jin B 2008 Ultrafast high-field carrier transport in GaAs measured by femtosecond pump-terahertz probe spectroscopy *Appl. Phys. Lett.* **93** 121115
- [36] Shu-shen L and Jian-bai X 1997 Effective-mass theory for InAs/GaAs strained superlattices *Acta Phys. Sin.* **6** 848
- [37] Hori Y, Ando Y, Miyamoto Y and Sugino O 1999 Effect of strain on band structure and electron transport in InAs *Solid State Electron.* **43** 1813–6